TAIL-ROTOR THRUST ON A 5.5-FOOT HELICOPTER MODEL IN GROUND EFFECT

R. Wayne Empey and Robert A. Ormiston
Ames Directorate
U. S. Army Air Mobility R&D Laboratory
Moffett Field, California 94035

PRESENTED AT THE 30th ANNUAL NATIONAL FORUM
OF THE
AMERICAN HELICOPTER SOCIETY
WASHINGTON, D.C.
MAY 1974

PREPRINT NO. 802

TAIL-ROTOR THRUST ON A 5.5-FOOT HELICOPTER MODEL IN GROUND EFFECT

R. Wayne Empey and Robert A. Ormiston
Research Scientists
Ames Directorate
U. S. Army Air Mobility R&D Laboratory
Moffett Field, California 94035

Abstract

Wind-tunnel experiments were conducted to investigate tail-rotor performance for flight conditions in ground effect where helicopter directional control deficiencies have been experienced. Tail-rotor thrust was measured on a small-scale helicopter model for various wind speeds and azimuths. Measurements were made with the fuselage and fin removed to emphasize the primary interference effects of a main rotor in ground effect. For a main-rotor height/diameter ratio h/D = 0.265, the largest thrust reductions occur when (i) the tail rotor rotates in the direction where the top blade moves forward, (ii) wind speeds are above 15 knots, and (iii) wind-azimuths are between 50° and 180°. Opposite rotation of the tail rotor eliminates most of the adverse interference effects of the main rotor. Flow visualization with neutrally buoyant helium bubbles revealed a small, well-defined ground vortex core at moderate and high wind velocities. Interpretation of the measured data showed that the ground vortex and trailing vortex systems of the main-rotor flow field produced tail-rotor thrust perturbations that are due to rotational and axial interference with the tail rotor.

Notation

b	number of blades
c	blade chord, ft
C_T	rotor thrust coefficient, $T/\rho\pi\Omega^2 R^4$
D	main rotor diameter, ft
h	main rotor height above ground, ft
r	radial distance from rotor center, ft
R	rotor radius
T	rotor thrust; tail-rotor thrust is positive in a counterclockwise direction around main rotor shaft, looking down on model
TA	tail rotor rotation direction where top blade moves aft
TF	tail rotor rotation direction where top blade moves forward
V	wind velocity or free-stream velocity, knots
V_T	rotor-tip speed, ft/sec
β	wind azimuth angle or vehicle sideslip angle, positive nose left, degrees (see Fig. 9)
θ	rotor-blade pitch angle, r/R = 0.75, deg
μ	main rotor advance ratio, $V/R\Omega$
ρ	air density, slugs/ft^3
σ	solidity, $bc/\pi R$
Ω	rotor angular velocity, rad/sec

Single-rotor helicopters generally employ a tail rotor for torque reaction and directional control. The highly variable aerodynamic environment of the tail rotor often leads to undesirable directional control characteristics, particularly for crosswind conditions in ground effect. Recent experience with these problems[1,2] has stimulated research to determine the cause of reduced tail-rotor thrust to improve fundamental knowledge of aerodynamic phenomena peculiar to the main- and tail-rotor system in ground effect.

Some of the earliest research by Amer and Gessow[3] provided analytical methods for predicting tail-rotor thrust for sideslip angles up to 360° azimuth, including vortex ring conditions. However, the effects of tail-rotor/fin interference and the main-rotor wake in ground effect were not considered. A more recent summary of several significant tail-rotor aerodynamic phenomena is given by Lynn et al.[4] Effects of tail-rotor/fin interference including separation distance and tractor/pusher arrangements, vortex-ring conditions, airfoil section, disc loading, and tip speed were discussed. Only brief attention was given to tail-rotor rotation direction and ground effect.

Huston and Morris[5] were the first to clearly identify (in terms of its significance for tail-rotor interference) the basic recirculation vortex caused by a crosswind acting on the flow field of a main rotor in ground effect. This horseshoe-shaped "ground vortex" was found to strongly influence tail-rotor thrust and power of a small-scale model tested in a wind tunnel in rearward flight, with $\beta = 180°$. The ground vortex, initially in front of the rotor for low velocities, was forced downstream and into the region of the tail rotor as velocity increased. Tail-rotor thrust reductions occurred when the vortex and the rotor were coincident, and the rotational flow of the vortex reduced the relative angular velocity of the tail-rotor blades.

Additional insight into many aspects of tail-rotor performance was given by Weisner and Kohler[6], again for small-scale wind-tunnel model tests. The effect of the ground vortex was substantiated for $\beta = 180°$, and its effect was noted for other azimuths at higher velocities. A significant influence of the main-rotor trailing vortex system on the tail-rotor thrust was also found. The effects of main-rotor height, tail-rotor position, rotation direction, tail-rotor/fin interference, and tractor-pusher arrangements were also investigated. Most recently Yeager et al.[7] expanded the work of Ref. 5 to investigate different wind-azimuth conditions and the important effects of tail-rotor/fin interference.

These small-scale model tests[5-7] contributed greatly in identifying conditions of reduced tail-rotor performance and in understanding the fundamental aerodynamic phenomena involved. However, because of the complex flow-field interference and the large number of system parameters, more experimental tests were needed. For example, Ref. 5 includes data for only one wind-azimuth, $\beta = 180°$, one main-rotor height, h/D = 0.355, and one tail-rotor rotation direction, TF. Reference 6 includes data for a large but incomplete wind-azimuth range, $0° < \beta < 270°$, one tail-rotor pitch angle, $\theta = 20°$, only high wind velocities, 20 and 35 knots, and two main-rotor height/diameter ratios, h/D = 0.3 and 1.0. Reference 7 presents

Presented at the 30th Annual National Forum of the American Helicopter Society, May 7–9, 1974.

data, usually including the effects of the fuselage and fin, for a complete range of wind velocity and azimuth, both tail-rotor rotation directions, and one main-rotor height/diameter ratio, h/D = 0.355. Most of the results from these experiments were obtained for a complete helicopter configuration that included a fuselage and tail fin. Since no complete series of tests was conducted for a main- and tail-rotor alone, these results are difficult to interpret with regard to the basic aerodynamic interference phenomena of the main- and tail-rotor combination.

The present experiments were designed to focus specifically on the fundamental aerodynamic phenomena. Comprehensive measurements of tail-rotor thrust were made for a complete range of the basic system parameters such as wind velocity, wind-azimuth, tail-rotor collective pitch, and tail-rotor rotation direction. Measurements were made only for the main- and tail-rotor combination. Less important effects of the fuselage and tail fin were not considered. Flow visualization studies of the aerodynamic phenomena were also carried out. The results were intended to be sufficiently general for use in future validation of analytical models of the main- and tail-rotor flow field.

Model and Test Procedure

A 1/8-scale model of the AH-1G Cobra helicopter was tested in the settling chamber of the USAAMRDL – Ames Directorate 7-by 10-Ft Wind-Tunnel. The principal model parameters and dimensions are given in Table 1. Side and plan views are shown in Fig. 1. In order to simplify the model, teetering hinges and cyclic pitch controls were not installed. The main- and tail-rotor blades were rigidly attached to their respective hubs, except that pitch changes could be made manually by loosening the hub clamps. The lack of a teetering hinge does produce asymmetric rotor loading in forward flight; but at very low advance ratios near hover, the asymmetry is not considered to be important. The fuselage and fin of the model were used for flow visualization studies, but were removed for quantitative testing.

The model was mounted on a 12- by 16-ft ground plane, 1 ft above the floor of the wind-tunnel settling chamber. The large size (30-ft high, 33-ft wide) of the settling chamber was sufficient to eliminate any perceptible wind-tunnel wall effects even for very low speed conditions. The model could be rotated through the entire 360° azimuth range. The tail rotor was powered by an electric motor driving a shaft through a straight tubular cantilever support. The tail-rotor and its support system were mounted external to the fuselage in order to simplify the drive train. This apparatus could be positioned on either side of the model to avoid wake interference with the tail rotor for certain azimuth angles. The general arrangement of the model installation in the wind tunnel is shown in Fig. 2. The height of the model could be changed by raising the rotor supports as shown in Fig. 3. Note that the fuselage and fin have also been removed in this figure. The main and tail rotors were instrumented with strain gages to measure thrust forces. The strain gage output was filtered to eliminate high-frequency turbulence response, and thus the measurements reflect only the steady state time-averaged rotor forces.

Data were obtained for the complete wind-azimuth range. Free-stream velocities varied from 0 to 44 knots (all velocities refer to full-scale values). The model was originally designed to operate at full-scale tip speeds but the rotor speeds were arbitrarily reduced to improve model reliability. The nominal tip speeds were 70% of the full-scale values (see Table 1), and the tunnel velocities were reduced proportionately to maintain the same main-rotor advance ratio for the model and full-scale conditions. Advance ratio varied from 0 to about 0.1. Maximum tunnel velocity was reached at an advance ratio of 0.05, and higher advance ratios were attained by reducing the rotor tip speeds below the nominal 70% values. The bulk of the testing was carried out with the model at skid height (h/D = 0.265), but a few measurements were made at h/D = 0.493. At skid height, the main-rotor-blade pitch angle was set at 5.83° for all velocities. This pitch angle represents a full-scale rotor thrust of 9000 lb, or $C_T = 0.00442$. At the higher advance ratios, the thrust coefficient increased slightly to $C_T = 0.00523$ at a velocity of 30.9 knots. Since the fine pitch variations required at these low speeds could not be made accurately, the small variations in rotor thrust were accepted. For h/D = 0.493, the rotor pitch angle was increased by 1° to maintain approximately the same rotor thrust.

Two tail-rotor rotation directions were used for testing with the main rotor. The rotation direction is referred to as TF or TA, depending on whether the blade at the top of the tail rotor disc moves forward toward the nose of the helicopter or aft toward the tail, respectively. Only the standard AH-1G configuration of relative main- and tail-rotor position was tested, although with the fuselage and fin removed, the tail-rotor disc was positioned to coincide with the "fuselage" plane of symmetry.

Flow Visualization

Smoke and neutrally buoyant helium soap bubble flow visualization techniques were used to investigate the main-rotor and tail-rotor flow fields. Free-stream and rotor-tip velocities were reduced to 20% of the full-scale values to reduce smoke and bubble dissipation and improve photography. There were, however, no noticeable changes in the flow-field phenomena at these very low velocities and Reynolds numbers. The smoke technique was adequate for observing large-scale flow-field behavior and was suitable for motion picture filming, but the smoke technique did not reveal fine details of the flow and was not adequate for still photography. The neutrally buoyant helium bubble technique, using the Sage Action, Inc., Model 3 Bubble Generator, was very successful, however, and revealed small details of the flow-field. Still photographs of the bubbles were easily obtained, but motion picture filming required careful attention to details of lighting and exposure.

A series of photographs with the helium bubbles shown in Fig. 4 illustrates the evolution of the main-rotor flow-field and the ground vortex as the free-stream velocity increases from 9.7 to 26.5 knots. At very low speeds, the rotor downwash extends far upstream of the rotor until it is overcome by the free-stream velocity and is swept back down-stream to recirculate through the rotor. The forward stagnation line between the rotor downwash and the free-stream flow moves rearward with increasing free-stream velocity as the recirculation region becomes smaller and the velocities more intense. When the stagnation line nears the leading edge of the rotor (at 19.9 knots), it becomes unstable, and the recirculating flow, or ground vortex, tends to oscillate between two different positions. At V = 21.9 knots, the structure of the ground vortex changes and a definite vortex

core begins to appear below the rotor leading edge. As the free-stream velocity increases, the core diameter becomes very small and well defined. The approximate position (based on visual estimation) of the ground vortex forward stagnation line for various free-stream velocities is shown in Fig. 5 (at the higher speeds the vortex core location is given). It is of particular interest to note the azimuth position where the vortex core and the rotor perimeter coincide, because this also indicates where the vortex will be in close proximity to the tail rotor. Figure 6 is a crossplot showing the ground vortex stagnation point (at the rotor centerline) as a function of free-stream velocity. The discontinuity at 19.9 knots is associated with the unstable vortex position behavior observed during the tests.

The well-defined core structure of the ground vortex observed during the present investigation was not reported in earlier work, and it is useful to note its basic characteristics, (for $h/D = 0.265$ and $C_T \cong 0.00442$). Below 22 knots, the ground vortex is characterized by relatively diffuse circulatory flow. At higher speeds, the circulatory flow became very similar to an ideal potential vortex. The photograph for 24.3 knots in Fig. 4 shows the fully developed vortex core with a diameter on the order of the bubble size, i.e., about 1/4 to 1/2 in., at the rotor centerline. The larger apparent diameter is caused by unsteady motion of the core during the 1-second-exposure interval. Note that in this photograph the bubbles are injected directly into the vortex core about two feet to the left of the rotor centerline. The bubbles migrate laterally upstream and cross the main-rotor centerline to occupy the entire vortex core, which extends just beyond each side of the rotor disc perimeter. The bubbles oscillate laterally within the vortex core and eventually exit from the core at either side and are swept downstream. Bubbles remain in the vortex core for up to 10 seconds after bubble injection is stopped. At either side of the rotor, the vortex core expands and becomes diffuse, turbulent, and very unsteady (just beyond the bubble injector, Fig. 4e). This behavior suggests a type of vortex bursting phenomenon. It may also be a region of transition between the ground vortex and a main-rotor trailing vortex system. Observation of bubbles being entrained into the vortex core suggests that the core may be the result of an accumulation of blade tip vortices deposited around the front of the rotor disc. The ends of the ground vortex core may be the points where the tip vortices no longer accumulate but are swept individually downstream.

In previous investigations[5-7] of tail-rotor performance, the fully developed ground vortex core structure was not observed, presumably because smoke and tuft grids were used for flow visualization. The vortex core is nearly invisible with smoke flow visualization, but it is clearly and easily observed with helium bubbles. Also no evidence of vertical vortices reported by Weisner and Kohler[6] was found in the present work. The helium bubble technique is especially suited to studies of the ground vortex because of the low-velocity circulatory flows, and because velocities tangent to the vortex core axis are very low. Therefore, bubbles entering the vortex core remain in a very localized region and clearly define the vortex behavior. The ground vortex core was also found to be sensitive to the presence of the fuselage. With the nose upwind, $\beta = 0°$, the fuselage substantially retarded the development of the small-diameter vortex core. Only a small effect was found for the tail upwind, $\beta = 180°$. And for the increased main-rotor height/diameter ratio, $h/D = 0.493$, the ground vortex core was found only at higher velocities and farther below the rotor.

Several photographs in Figs. 7 and 8 graphically show how the ground vortex core interacts with the tail rotor under certain critical crosswind conditions. Figure 7 shows the model positioned tail forward, $\beta = 180°$, at V = 15 knots, a critical condition (first identified by Huston and Morris[5]) when the tail-rotor rotation direction is the same as the ground vortex, i.e., TF rotation. Note that a comparison with Fig. 4b shows that, with the tail rotor operating at high thrust, the ground vortex moves downstream and is reduced in size. Figure 8a shows the model positioned in a 21.9 knots crosswind of $\beta = 90°$. Here, the vortex core is fully developed and it impinges directly on the fin and on the tail rotor. The core diameter appears to be enlarged due to unsteady flow, and the vortex oscillates between the leading and trailing edges of the fin. Figures 8b and 8c show that a change in wind azimuth of 20° is sufficient to prevent direct impingement of the vortex core on the tail rotor. This is true even in Fig. 8c where an increased speed of 26.5 knots would tend to reduce the separation distance between the tail-rotor and the ground vortex.

Test Results

A few experimental results are presented to illustrate the general thrust performance characteristics of a tail rotor in the presence of a main rotor operating in ground effect at low forward speeds.

First shown in Fig. 9 is tail-rotor thrust versus azimuth for a series of tail-rotor pitch angles from 0° to 18°, at a wind velocity of 21.9 knots. Three separate configurations are included: (i) the tail rotor alone (Fig. 9a); (ii) the tail rotor with the TF-rotation direction, together with the main rotor (Fig. 9b); and (iii) the tail rotor with the TA-rotation direction, together with the main rotor (Fig. 9c). Figure 9a, for the tail rotor alone, shows the basic thrust variations which occur when a rotor experiences an angle-of-attack variation from 0° of 360°. The rotor is in axial flow in the normal working state (propellor) at $\beta = 90°$ and in the vortex-ring state at 270°. At $\beta = 0°$ and 180°, the rotor is in edgewise flow, i.e., as a lifting rotor. The largest thrust reduction occurs for $\beta = 90°$ because the wind increases the rotor inflow. In the vortex-ring state, $\beta \cong 270°$, significant unsteady perturbations occur, which contribute to difficulties in helicopter directional control. To indicate how the main-rotor flow field and the tail-rotor rotation direction influence the tail-rotor thrust, Figs. 9b and 9c should be compared with Fig. 9a. At 21.9 knots, the ground vortex core is well-developed and is close to the tail rotor when $\beta \cong 90°$ or 270°. A large thrust reduction occurs at high pitch angles for TF-rotation when $\beta \cong 90°$ or 270°, because of the ground vortex interference. A much smaller change occurs for the TA-rotation direction, which implies that the rotation direction is an important factor for tail-rotor thrust performance in ground effect. However, the rotation effect is not the only interference effect produced by the main rotor. At low tail-rotor pitch angles, the main rotor significantly influences the tail-rotor thrust, but both rotation directions produce virtually identical results. Finally, the thrust measurements indirectly imply that the tail rotor itself influences the main rotor flow field. This is suggested in Fig. 9c by the azimuthal variation of the point of minimum thrust as the tail-rotor pitch is changed. The minimum thrust azimuth varies from 90° to 110° as the pitch angle varies from 18° to 0°. This would be expected if the ground vortex were induced further downstream (see Fig. 5) by the tail-rotor inflow.

Figure 10 shows the variation of tail-rotor thrust with free-stream velocity for four azimuth angles, $\beta = 0°, 90°, 180°$, and 270°. These results clearly show the effect of the ground vortex on tail-rotor thrust as it moves downstream with increasing velocity. For the headwind condition $\beta = 0°$ (Fig. 10a), the ground vortex is not a factor, but there is a rotational flow effect due to the partial immersion of the tail-rotor disc in the slipstream of the main rotor. Figure 10b shows again that, for $\beta = 180°$ and the TF-rotation direction, 15 knots is the critical velocity. The TA-rotation shows a small favorable interference effect from the ground vortex. Figures 10c and 10d show the crosswind conditions, and here the variations in tail-rotor thrust are more pronounced. At $\beta = 90°$ (Fig. 10c), the free-stream velocity reduces the rotor thrust because of the increased inflow, but the ground vortex causes a significant additional reduction at 22 knots. The vortex interference is only present for a restricted velocity range, which implies that interference effects occur only when the vortex is in close proximity to the tail rotor. An exception for zero pitch angle shows a thrust reduction at high velocities that is not a function of rotation direction. Figure 10d shows tail-rotor thrust in the vortex-ring condition, $\beta = 170°$. The thrust perturbations are correspondingly more complex; however, a reduction in thrust due to the ground vortex does occur near 22 knots at high tail-rotor pitch angles and the TF-rotation direction.

The influence of increased ground clearance of the main rotor was evaluated in a limited fashion (Fig. 11) for $\beta = 90°$. Comparison wth Fig. 10c shows clearly that the ground vortex effect at high pitch angles is completely absent. Some influence of the main rotor flow field are evident at the lower pitch angles, however.

Flow-Field Interpretation from Tail-Rotor Thrust Perturbations

Tail-rotor thrust perturbations that occur for a main- and tail-rotor configuration operating in a crosswind and in ground effect were discussed above. Although the rudimentary features of the associated aerodynamic phenomena are now known, a better understanding will be required before tail-rotor performance can be quantitatively determined or improved. The thrust data and flow-visualization observations reported herein can be interpreted to help understand these phenomena; the process used to gain this insight is described below.

Flow-Field Model

A flow-field model is first hypothesized for a rotor in ground effect at low forward velocities. The two main elements of this flow model are the ground vortex and the rotor trailing vortex system. The ground vortex system created by the recirculating rotor downwash has been directly identified by flow visualization but the trailing vortex system for these conditions is implied only indirectly by perturbations in tail-rotor thrust. The two vortex systems are shown schematically in Fig. 12. For the present main- and tail-rotor configuration and main-rotor height/diameter ratio $h/D = 0.265$, the ground vortex and the rotor trailing vortex system are below and above the tail-rotor hub, respectively. The details of how this vortex system is formed are not entirely clear, especially with respect to the "connections" between the ground and trailing vortex systems (Levinsky and Strand[8] have proposed a single, combined vortex model). Both systems must originate from the blade trailing tip vortices that are normally deposited in a continuous spiral pattern behind the rotor. However, in ground effect, the portions of the spiral that are deposited at the front of the rotor initially move upstream of the rotor and recirculate in the ground vortex. At higher speeds, it appears that they accumulate to form the well-defined core of the ground vortex. The portions of the blade tip vortices deposited at the sides and rear of the rotor are swept downstream in the normal manner and form a trailing vortex at each side of the rotor with interconnecting lateral filaments. An undetermined aspect of this vortex formation process is the point where the blade tip vortices "divide" to join either the ground vortex or the main-rotor trailing vortex system. This is an important point, because it determines the details of the trailing vortex configuration in the region where the trailing vortex exerts its greatest influence on the tail rotor.

Tail-Rotor/Vortex Interference

The second step in understanding the main- and tail-rotor aerodynamic phenomena is to determine whether the measured thrust perturbations due to the main rotor wake are consistent with the hypothesized vortex model. Tail-rotor thrust perturbations caused by an adjacent vortex (such as the ground vortex or the trailing vortices) can be divided into two types: rotational interference and axial interference.

Rotational Interference. Consider an ideal potential vortex that is parallel to the tail-rotor shaft (Fig. 13a) and induces a rotational flow in the same direction as the tail-rotor rotation. If the vortex is positioned outside the rotor perimeter, it will increase the relative blade rotational velocity and increase the rotor thrust. The thrust perturbation will increase as the vortex moves closer to the rotor (when the vortex is near or just within rotor perimeter, the thrust perturbation will be sensitive to assumptions about viscous vortex properties like core size, etc.). As the vortex approaches the rotor center, the thrust is reduced because the vortex rotation reduces the relative angular velocity of the blades. In summary, as the vortex traverses the rotor, the thrust is first increased and then decreased as the vortex approaches the center of the rotor. If the vortex rotates in a direction opposite to the rotor, generally opposite thrust perturbations occur, although the variation with position will not be identical. And finally, pure rotational interference will cause thrust perturbations only if the blade pitch angle is nonzero.

Axial Interference. The second basic type of thrust perturbation occurs if the vortex axis is perpendicular to the rotor shaft as shown in Fig. 13b. In this case, the velocity induced by the vortex in the axial direction with respect to the rotor (normal to the disc) will increase or decrease the rotor inflow, and hence decrease or increase the rotor thrust. The sign of the thrust perturbation depends on the vortex rotation direction. The thrust perturbation will become greater as the vortex approaches the edge of the rotor disc, and then will diminish to zero when the vortex coincides with the rotor axis. Axial interference is not substantially dependent on the rotor-blade pitch angle, or the rotor rotation direction.

The rotational and axial interference conditions are actually special cases of a more general oblique rotor/vortex interference condition. The oblique interference condition will be characterized by a combination of both rotational and axial interference effects.

Analysis of the Data

The ground and trailing vortex flow-field hypothesis and the rotor/vortex interactions (described above) are now used to study the tail-rotor thrust measurements. Figure 14a shows the tail-rotor thrust at zero pitch angle vs wind azimuth for the complete range of wind velocities tested. Superposition of the isolated tail rotor and the TA- and TF-rotation, main- and tail-rotor combinations clearly shows the influence of the main-rotor flow field and the tail-rotor rotation direction on the tail-rotor thrust. The sequence of curves for small wind velocity increments gives a graphic picture or "mapping" of the main-rotor flow pattern and its development as wind speed increases. For zero blade pitch angle, only axial interference thrust perturbations are expected; this is confirmed by the insensitivity of the thrust perturbations to tail-rotor rotation direction. Therefore, the thrust perturbation caused by the main-rotor can be used to qualitatively estimate the axial (with respect to the tail-rotor axis) velocity components of the main-rotor flow-field at the tail-rotor location. Since the tail-rotor thrust is nearly zero for zero pitch angle, the following observations apply to the undisturbed main-rotor flow-field.

For velocities below 17 knots (Fig. 14a) there are only small tail-rotor thrust perturbations. Although the diffuse ground vortex is coincident with the tail rotor at 15 knots, at zero pitch angle its rotational flow does not influence the thrust. The tail-rotor thrust perturbations at (A) imply that the flow approaching the main rotor is induced toward the center of the rotor (analogous to a potential sink), thus partly nullifying the lateral velocity component ($V \sin \beta$), experienced by the isolated tail rotor.

At higher velocities, 22 to 30 knots, the ground vortex moves below the main rotor. A significant thrust perturbation (B) occurs, negative for $\beta = 90°$ and positive for $\beta = 270°$.* This is due to axial interference produced by a downstream induced velocity component of the ground vortex and is to be expected because the ground vortex is located below the tail-rotor hub. The azimuth angle of the maximum thrust perturbation approaches 90° and 270° as the ground vortex moves downstream with increasing velocity (Fig. 5). The main-rotor trailing vortices apparently produce the thrust perturbations at (C), increasing the thrust at $\beta = 45°$ and decreasing it at $\beta = 315°$. This is due to an axial interference velocity component of the trailing vortices positioned above the tail-rotor hub for these azimuths. Their influence diminishes as velocity decreases, since trailing vortices would not be expected to form in ground effect at very low speeds. At 20 to 22 knots, a thrust perturbation (D) can be observed for which there is no satisfactory explanation. And, finally, a small increase in thrust (E) at the downstream point of the main-rotor, $\beta = 360°$, is produced by the wake swirl reaction to the main-rotor torque.

Figures 14b and 14c show similar results for a tail-rotor pitch angle of 18°. Since rotational interference effects are produced for positive pitch, different thrust perturbations are found for the two tail-rotor rotation directions. Therefore, the results for TF- and TA-rotation are shown separately in Figs. 14b and 14c, respectively. Since the tail rotor is operating at high thrust, the main-rotor flow-field characteristics are also slightly different from those in Fig. 14a.

The results in Fig. 14b for TF-rotation generally show large thrust reductions that are characteristic of adverse rotational interference. The critical azimuth of about 180° at 15 knots changes continuously to about 50° as velocity increases to 30 knots. This reflects the downstream movement of the ground vortex with increasing velocity (Fig. 5). At very low velocities the thrust is reduced for all azimuths, because of rotational interference caused by partial immersion of the tail-rotor disc in the adjacent main-rotor slipstream At higher velocities, the ground vortex forms and creates the thrust perturbation at (F) (perturbation (B) in Fig. 14a).

The strongest ground vortex effect (F) occurs at $\beta = 90°$ for velocities of 20 to 24 knots. For these conditions, rotational interference and axial interference of the ground vortex combine to reduce the tail-rotor thrust. For $\beta = 270°$, the positive axial interference (Fig. 14a) overcomes negative rotational interference at moderate and high velocities, (F). Compared with Fig. 14a, however, the ground vortex thrust perturbations peak at lower azimuths because the ground vortex is displaced by interference of the thrusting tail-rotor.

The thrust perturbation of the trailing vortex (G) near $\beta = 60°$ appears to merge with the perturbation caused by the ground vortex, (F). The negative thrust reduction due to rotational interference (for TF-rotation) of the trailing vortex above the tail-rotor hub outweighs the thrust increase from axial interference (Fig. 14a, (C)), and yields a net reduction in tail-rotor thrust. For wind-azimuths near $\beta = 315°$, the trailing vortex again reduces the tail-rotor thrust (G) because of combined thrust reductions from axial and rotational interference (TF-rotation). Finally, one significant thrust perturbation (H) remains unexplained; it may result from a complex secondary flow effect of the tail-rotor wake.

Figure 14e shows the effect of the main-rotor flow on tail-rotor thrust for TA-rotation. As noted above, and also in earlier work, this rotation direction nearly eliminates the adverse effect of the main-rotor flow field. This is due to the favorable rotational interference effect of the ground vortex on the tail rotor. This is also true for rotational interference of the trailing vortices for the present tail-rotor configuration. The TA-rotation direction does not completely eliminate the adverse tail-rotor thrust perturbation, however, because axial interference of the ground and trailing vortices can also reduce thrust.

Beginning at the low wind velocities in Fig. 14c, the increase in thrust due to rotational interference for TA-rotation evident at (I) is opposite the effect of TF-rotation at (F) in Fig. 14b. As the ground vortex moves under the main rotor at higher velocities, the largest thrust perturbations occur near $\beta = 90°$ or 270°. In region (I) for $\beta = 90°$, the adverse axial interference outweighs the favorable rotation interference. The net thrust reduction is not large, however. The two interference effects are both positive at $\beta = 270°$, and the tail-rotor thrust is increased. Finally, the trailing vortex effect at high velocities (J) increases the thrust at both $\beta = 45°$ and 330°, since the rotational interference outweighs the adverse axial interference near $\beta = 330°$.

*For this discussion, it will be useful to consider the free-stream velocity vector and the vortex systems to be fixed in space. The azimuth angle of the tail rotor, measured counterclockwise from the downstream position (Fig. 12), is then equal to the wind-azimuth angle β.

Concluding Remarks

The tail-rotor thrust performance characteristics of a small-scale helicopter model tested in a wind tunnel in ground effect generally agreed with the findings of earlier investigations; however, additional details are available from the present tests. The flow-visualization investigations revealed significant additional details of the ground vortex not reported by earlier investigators. Specific findings are listed as follows:

1. For a main-rotor height/diameter ratio h/D = 0.265 and $C_T \cong 0.0044$, tail-rotor thrust was substantially reduced for TF-rotation at high tail-rotor pitch angles, for nearly all wind velocities and azimuths. Thrust perturbations were smaller and usually favorable for TA-rotation.

2. For a main-rotor height/diameter ratio h/D = 0.265, $C_T \cong 0.0044$, and TF-rotation, the most critical thrust reductions occurred for wind velocity and azimuth combinations that varied continuously from 15.0 knots and 150° (similar to Huston and Morris[5]) to 30.9 knots and 50° as the ground vortex location changed with increased velocity. Minimum thrust occurred at 22 knots and 90°.

3. Limited results for a main-rotor height/diameter ratio h/D = 0.493 and $\beta = 90°$ showed no appreciable reductions in tail-rotor thrust.

4. Tail-rotor thrust measurements support Weisner and Kohler's finding that a main-rotor-tip vortex system causes tail-rotor thrust perturbations at moderate and high velocities at azimuth angles near 45° and 315°.

5. The neutrally buoyant helium bubble flow visualization technique was found to be ideal for studying the flow field of a main-rotor in ground effect. Use of this technique revealed that for velocities above 22 knots, the ground vortex possessed a very small well-defined core, 1/4 to 1/2 in. in diameter.

6. Detailed analysis of tail-rotor thrust perturbations caused by the main-rotor flow field at high and low tail-rotor pitch angles showed that thrust perturbations are caused by a combination of two basic types of rotor/vortex interference. The first is rotational interference due to a vortex parallel to the rotor shaft, and the second is axial interference caused by a vortex perpendicular to the rotor shaft.

7. Flow visualization and tail-rotor thrust measurements both showed that the tail-rotor can significantly alter the main-rotor flow field.

References

1. Lewis II, R. B., ARMY HELICOPTER PERFORMANCE TRENDS, Journal of the American Helicopter Society, Vol. 17, No. 2, April 1972.

2. Johnston, J. F., and Cook, J. R., AH–56A VEHICLE DEVELOPMENT, Paper presented at the 27th Annual National Forum of the American Helicopter Society, Preprint No. 574, Washington, D. C., May 1971.

3. Amer, K. B., and Gessow, A., CHARTS FOR ESTIMATING TAIL-ROTOR CONTRIBUTION TO HELICOPTER DIRECTIONAL STABILITY AND CONTROL IN LOW-SPEED FLIGHT, NACA Report TR 1216, 1955.

4. Lynn, R. R., Robinson, F. D., Batra, N. N., and Duhon, J. M., TAIL ROTOR DESIGN PART I: AERODYNAMICS, Journal of American Helicopter Society, Vol. 15, No. 4, October 1970.

5. Huston, R. J., and Morris, C. E. K., Jr., A WIND-TUNNEL INVESTIGATION OF HELICOPTER DIRECTIONAL CONTROL IN REARWARD FLIGHT IN GROUND EFFECT, NASA TN D-6118, March 1971.

6. Wiesner, W., and Kohler, G., TAIL ROTOR PERFORMANCE IN PRESENCE OF MAIN ROTOR, GROUND, AND WINDS, Paper presented at the 29th Annual National Forum of the American Helicopter Society, Preprint No. 764, May 1973.

7. Yeager, W. T., Jr., Young, W. H., Jr., and Mantay, W. R., A WIND-TUNNEL INVESTIGATION OF PARAMETERS AFFECTING HELICOPTER DIRECTIONAL CONTROL IN LOW-SPEED FLIGHT IN GROUND EFFECT, NASA Technical report (to be published).

8. Levinsky, E. S., and Strand, T., A METHOD FOR CALCULATING HELICOPTER VORTEX PATHS AND WAKE VELOCITIES, Air Force Flight Dynamics Laboratory Technical Report AFFDL-TR-69-113, July 1970.

Table 1. Model Parameters

	Main Rotor	Tail Rotor
Number of blades		2
Diameter, ft		1.061
Chord, ft		0.0875
Solidity		0.1051
Blade root cutout, percent		27.2
Blade twist, deg		0
Airfoil		NACA 0021 at r/R = 0.271 NACA 0008 at r/R = 1.0
Rotor-tip speed (100% rpm) ft/sec	746	736
Precone, deg	2.5	0

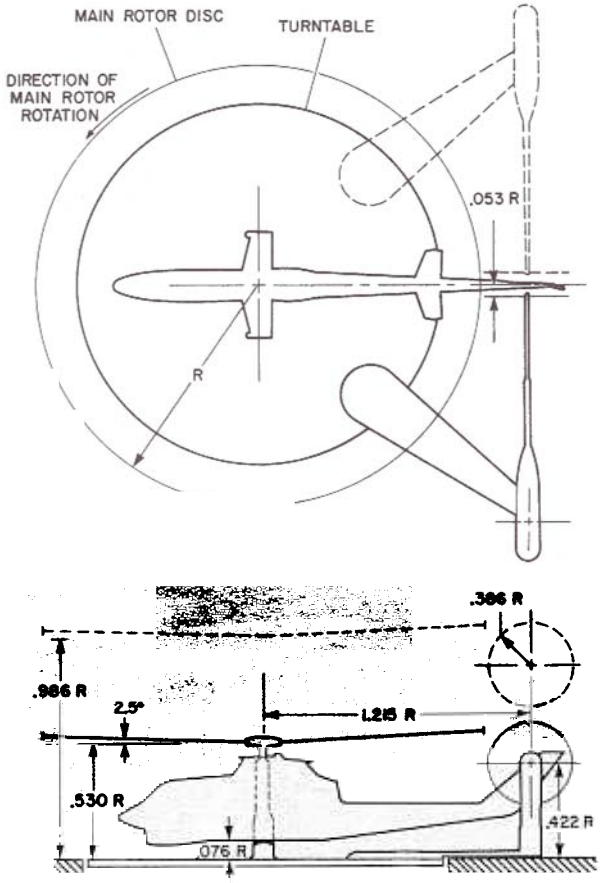

Fig. 1 AH-1G Cobra 1/8-scale wind-tunnel model, side and plan views, R = 2.75 ft.

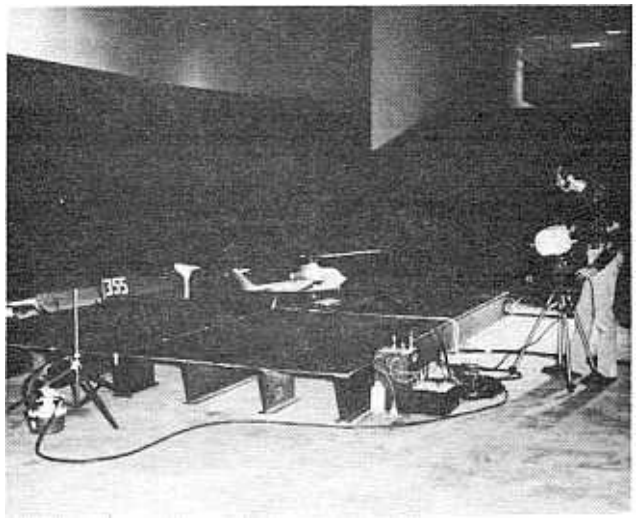

Fig. 2 Model installation in settling chamber of AMRDL-Ames 7- by 10-ft wind tunnel.

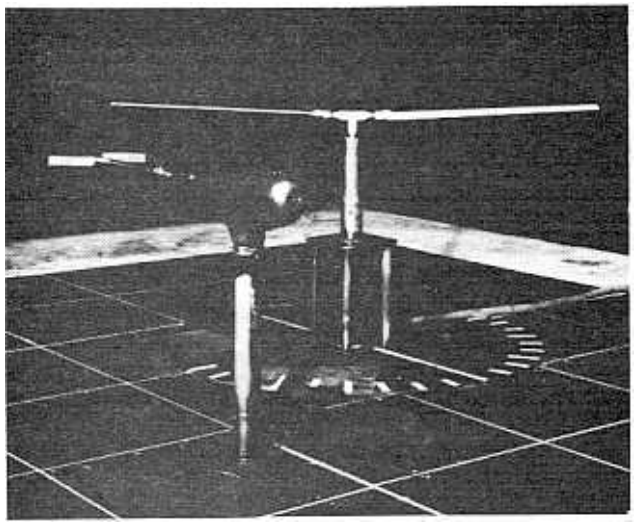

Fig. 3 Fuselage and fin removed, main rotor raised to ground height to diameter ratio h/D = 0.493.

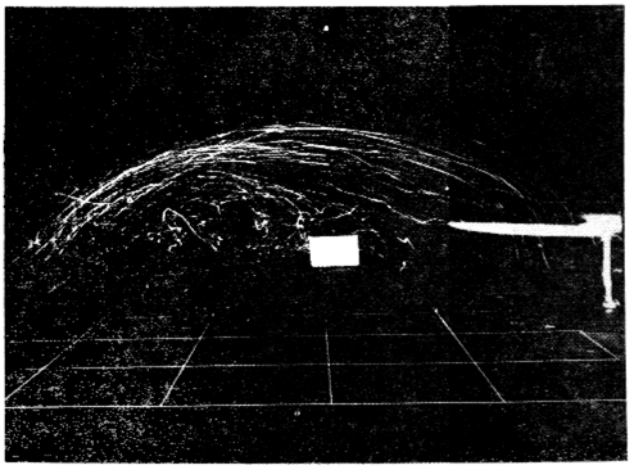

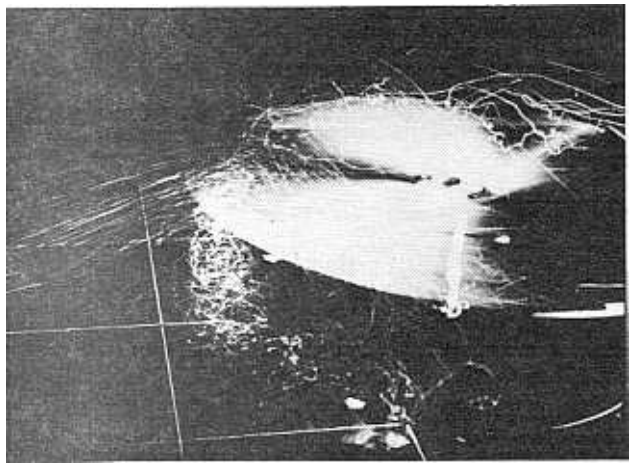

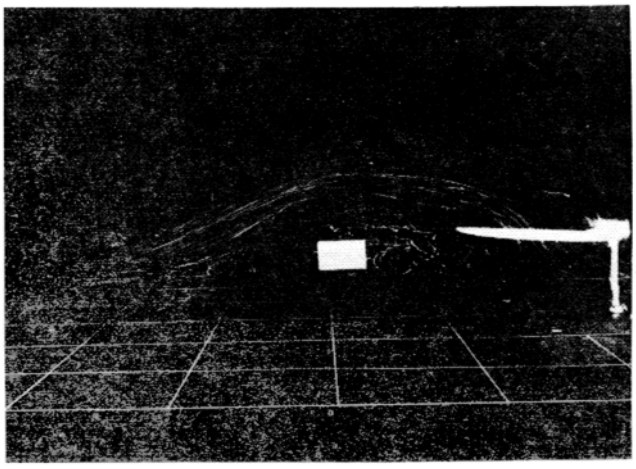

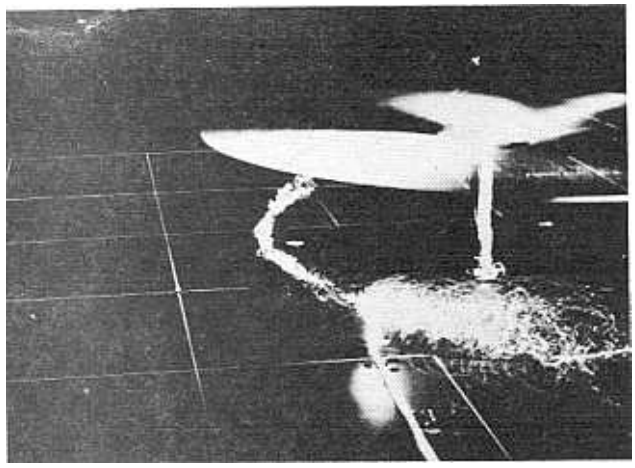

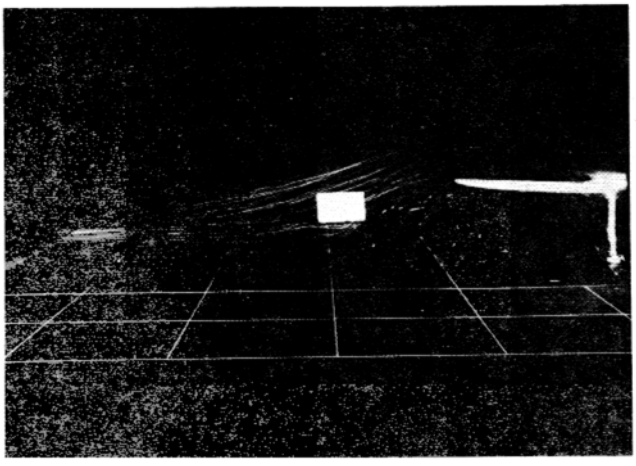

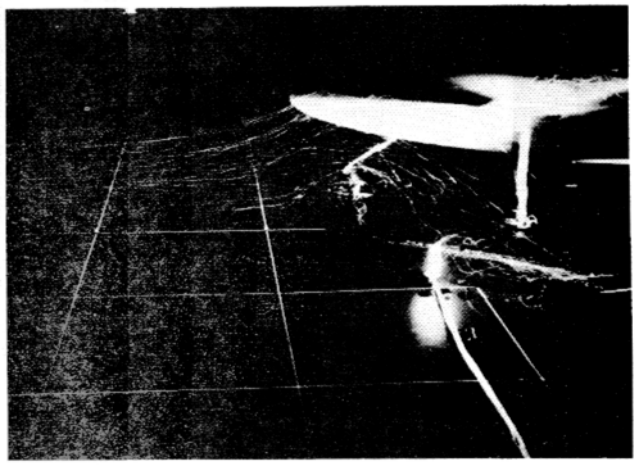

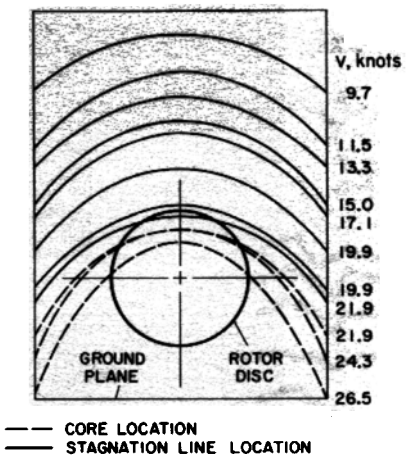

Fig. 5 Approximate position of ground vortex forward stagnation line, top view of ground plane, h/D = 0.265.

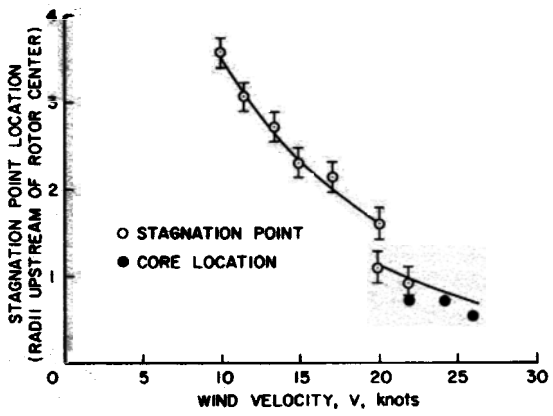

Fig. 6 Variation of ground vortex position at the rotor centerline vs free-stream velocity, h/D = 0.265.

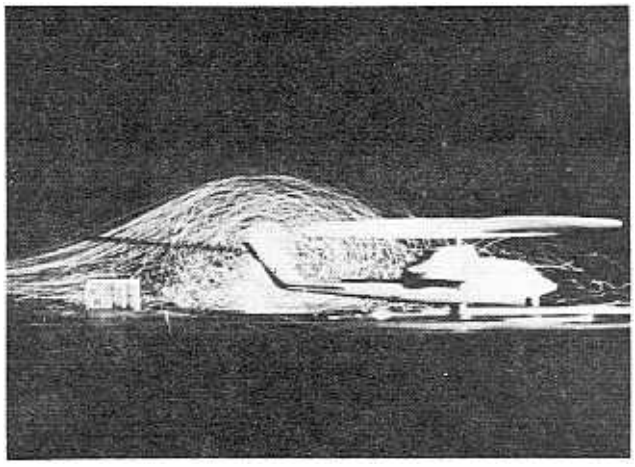

Fig. 7 Relative location of ground vortex and tail rotor, h/D = 0.265, $\beta = 180°$, V = 15.0 knots, tail-rotor pitch angle 18°.

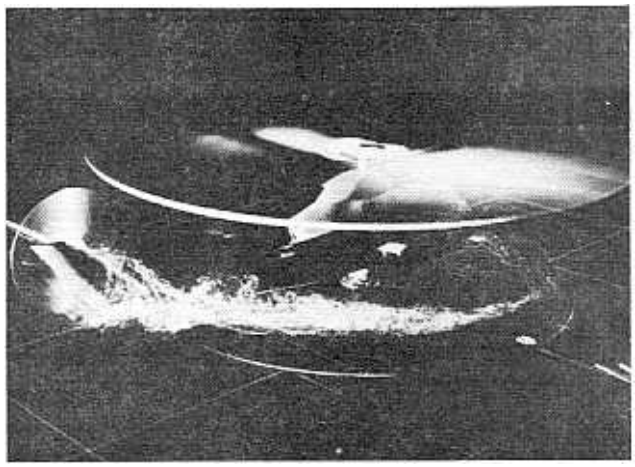

a) $\beta = 90°$

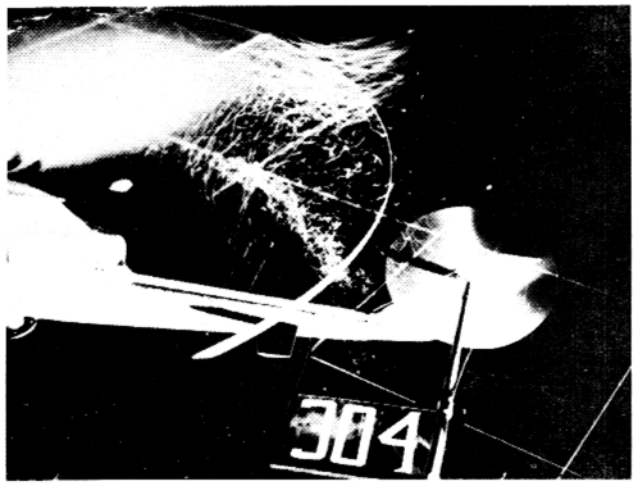

b) $\beta = 110°$

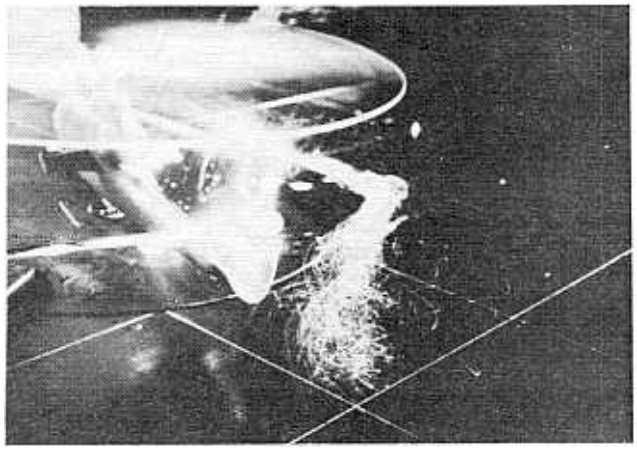

c) $\beta = 70°$, V = 26.5 knots

Fig. 8 Relative location of ground vortex and tail rotor, h/D = 0.265, V = 21.9 knots, tail-rotor pitch angle 18°.

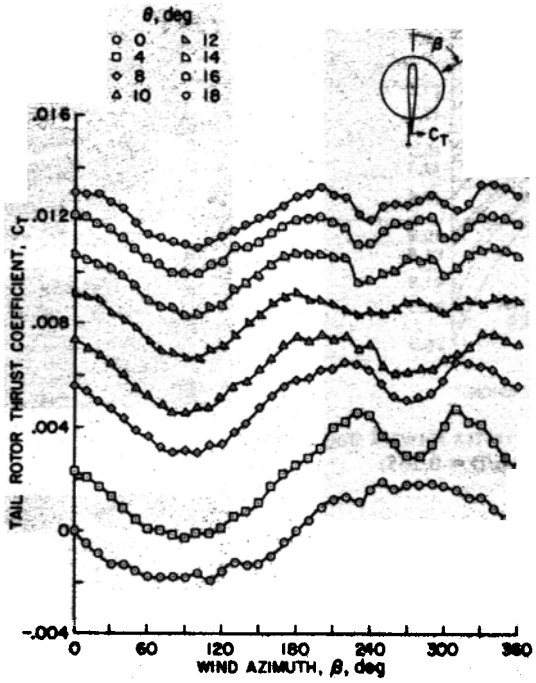

a) Without main rotor

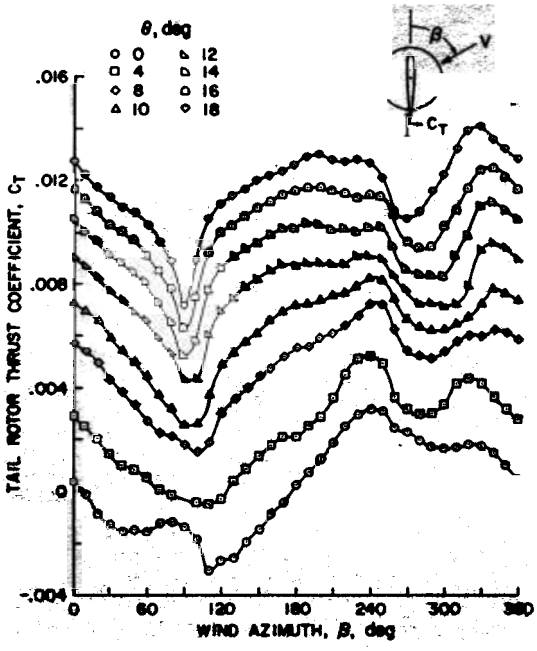

b) TF tail-rotor rotation direction

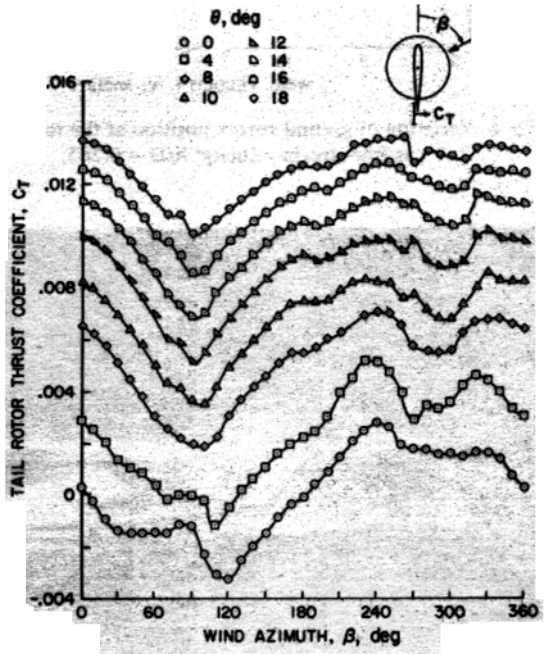

c) TA tail-rotor rotation direction

Fig. 9 Tail-rotor thrust coefficient vs wind-azimuth angle, h/D = 0.265, V = 21.9 knots, fuselage and fin removed.

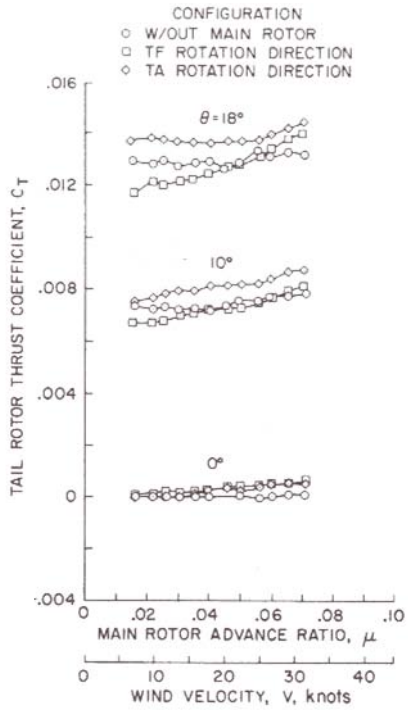

a) $\beta = 0°$

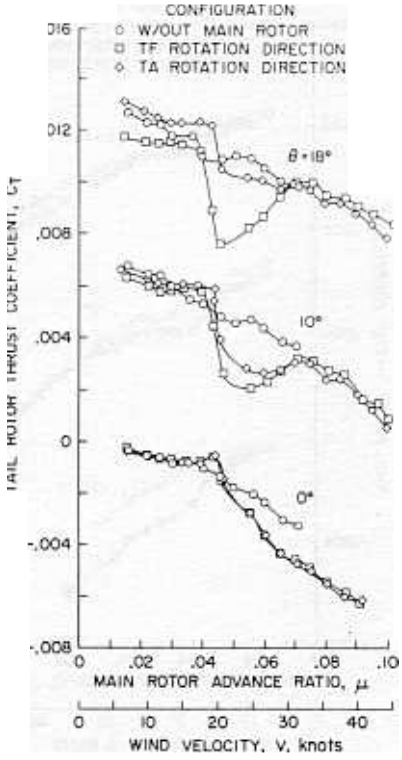

c) $\beta = 90°$

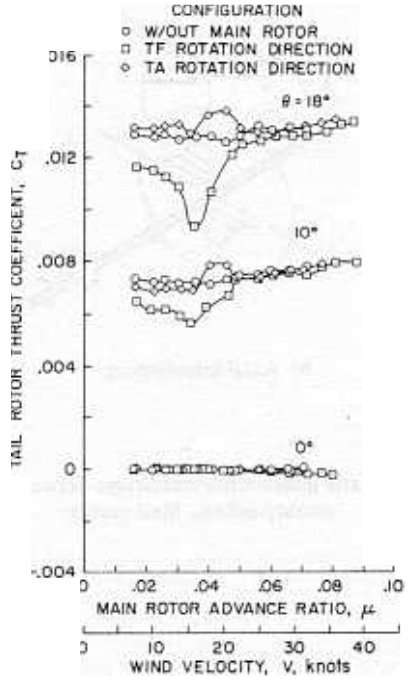

b) $\beta = 180°$

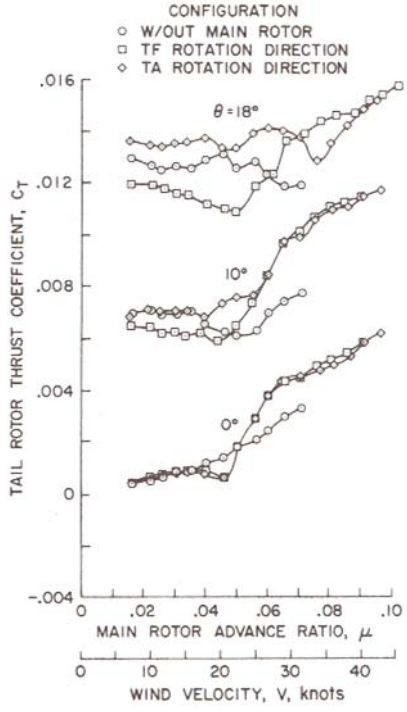

d) $\beta = 270°$

Fig. 10 Tail-rotor thrust coefficient vs wind velocity, h/D = 0.265, fuselage and fin removed.

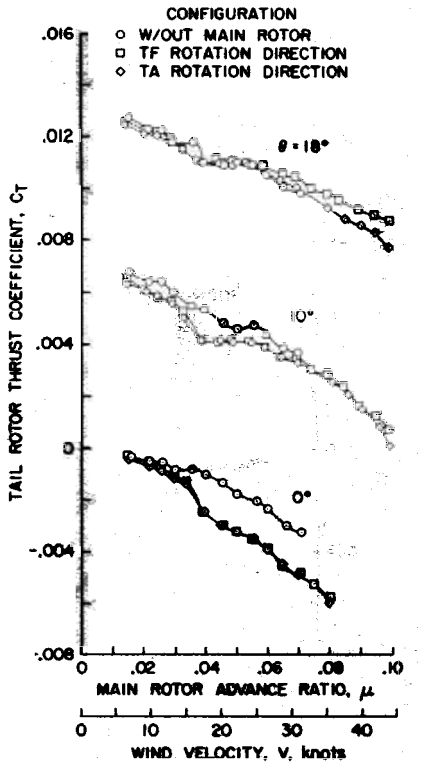

Fig. 11 Tail-rotor thrust coefficient vs wind velocity, h/D = 0.493, $\beta = 90°$, fuselage and fin removed.

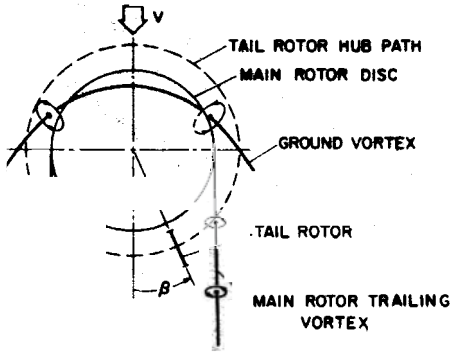

Fig. 12 Main-rotor flow-field model, top view showing ground vortex and trailing vortex systems.

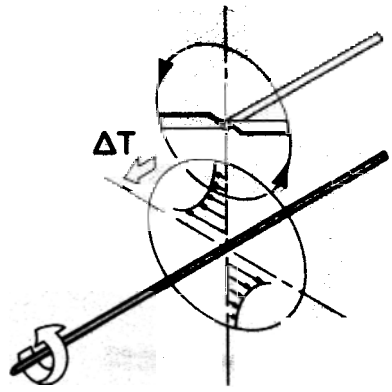

a) Rotational interference

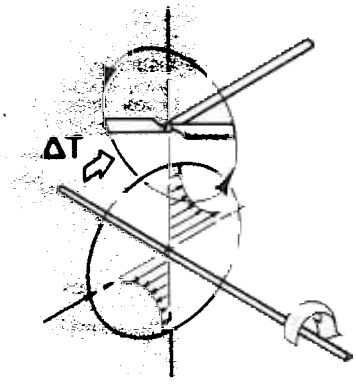

b) Axial interference

Fig. 13 Schematic interference conditions between a rotor and a doubly-infinite ideal vortex.

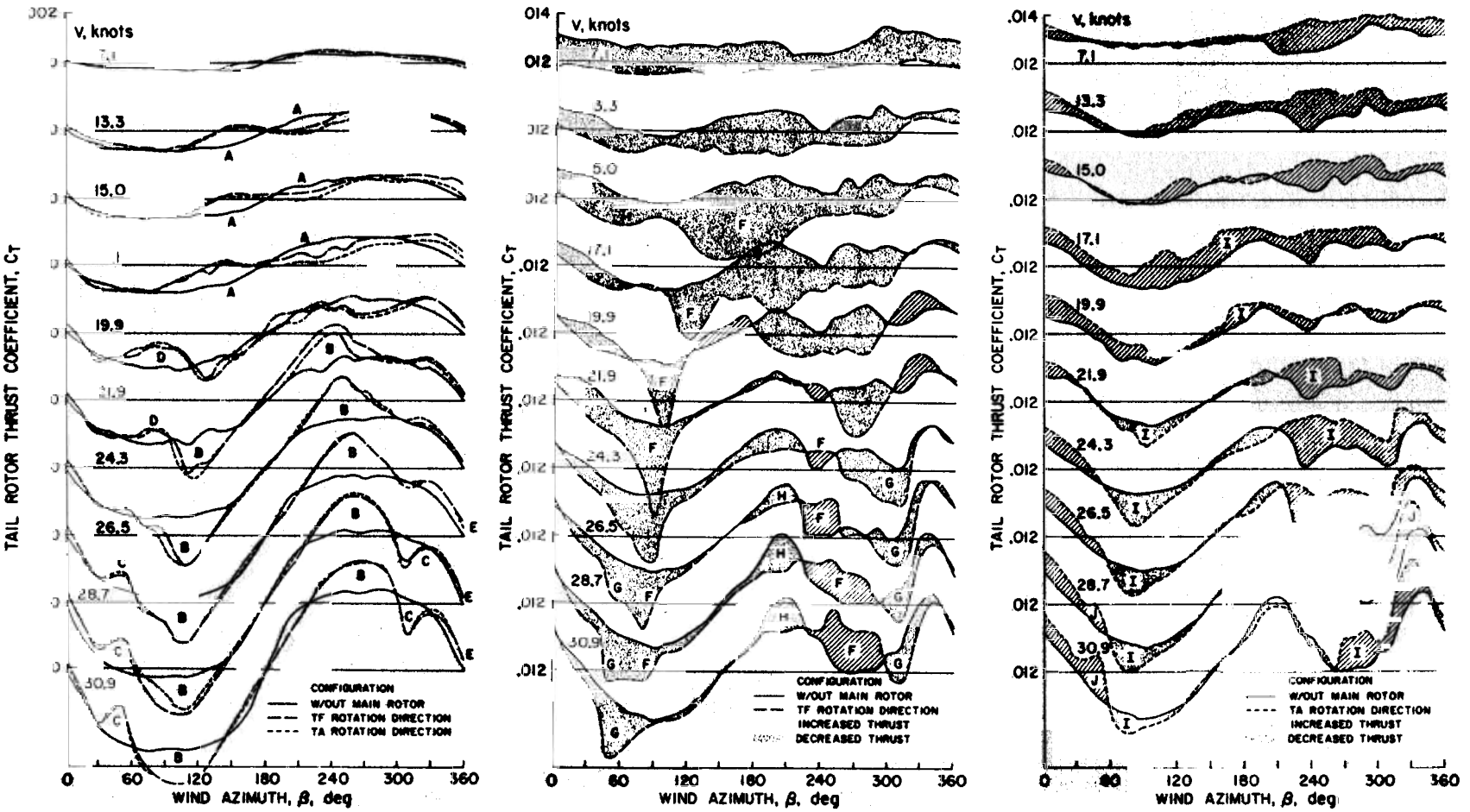

a) Tail-rotor pitch angle 0°

b) Tail-rotor pitch angle 18°, TF-rotation direction

c) Tail-rotor pitch angle 18°, TA-rotation direction

Fig. 14 Tail-rotor thrust coefficient vs wind-azimuth angle, h/D = 0.265, fuselage and fin removed.